

Information-guided pixel augmentation for pixel-wise contrastive learning

Quan Quan¹ Qingsong Yao¹ Jun Li¹ S.Kevin Zhou^{2,1}

¹ Key Lab of Intelligent Information Processing of Chinese Academy of Sciences (CAS), Institute of Computing Technology

² University of Science and Technology of China

Abstract

Contrastive learning (CL) is a form of self-supervised learning and has been widely used for various tasks. Different from widely studied instance-level contrastive learning, pixel-wise contrastive learning mainly helps with pixel-wise tasks such as medical landmark detection. The counterpart to an instance in instance-level CL is a pixel, along with its neighboring context, in pixel-wise CL. Aiming to build better feature representation, there is a vast literature about designing instance augmentation strategies for instance-level CL; but there is little similar work on pixel augmentation for pixel-wise CL with a pixel granularity. In this paper, we attempt to bridge this gap. We first classify a pixel into three categories, namely low-, medium-, and high-informative, based on the information quantity the pixel contains. Inspired by the “InfoMin” principle, we then design separate augmentation strategies for each category in terms of augmentation intensity and sampling ratio. Extensive experiments validate that our **information-guided pixel augmentation** strategy succeeds in encoding more discriminative representations and surpassing other competitive approaches in unsupervised local feature matching. Furthermore, our pretrained model improves the performance of both one-shot and fully supervised models. To the best of our knowledge, we are the first to propose a pixel augmentation method with a pixel granularity for enhancing unsupervised pixel-wise contrastive learning.

1. Introduction

Contrastive learning (CL) is a form of self-supervised learning (SSL), where data provides supervision via utilizing proxy tasks [8]. Compared with previous SSL approaches, contrastive learning focuses on learning representations of data in the embedding space by contrasting samples with the same and different distributions [4–6, 14]. Currently, it has been widely applied to boost the performance of classification, a typical instance-level task. However, when applying instance-level CL for pixel-level down-

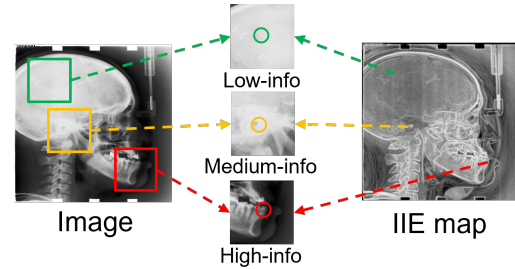


Figure 1. **Main idea:** the pixels are clustered into three classes: low-, medium-, high-informative, and each class is supplemented by corresponding strategy. IIE: image information entropy.

stream tasks [22, 53], e.g., landmark detection, segmentation, and object detection, it offers limited help when transferring instance-level contrastive learning methods to pixel-level downstream tasks directly, due to the discrepancy of supervision granularity. As a result, researchers plagued by pixel-level downstream tasks prefer pixel-wise CL.

The performance of pixel-wise CL largely depends on the generation of positive and negative pairs, which motivates us to think of such a challenge: *how to augment the training pairs for pixel-wise CL effectively?* Tian *et al.* [32] gives their answer for instance-level CL. They propose the so-called “InfoMin” principle: A good positive pair of images should share the minimal information necessary to perform well in the downstream task [32]. Tian *et al.* [32] argue that learning representations which throw out information about nuisance variables is preferable as it can improve generalization and decrease sample complexity on downstream tasks. Additionally, the optimal augmentation depends on the minimal shared information [32], which serves as inspiration and motivation for us to construct an “optimal” augmentation in pixel-wise CL.

In this paper, we aim to tackle this challenge by unveiling the advantage and characteristics of pixel-wise CL, and optimizing the acquisition of positive and negative pairs *with a pixel granularity* in an unsupervised style.

First, images are signals with unbalanced information

quantity at the pixel level. Each pixel with its context offers aids with varying degrees for the understanding of parts, objects and structures in an image. As a typical pixel-wise task, landmark detection usually benefits more from informative pixels. Therefore, measuring information of pixels within an image and concentrating more on informative regions will be helpful. A practical solution to achieve this is to introduce the knowledge from annotations [23, 37], *e.g.* Liu *et al.* [23] train a semi-supervised model to generate confidence maps where the pixels with high confidence are more involved in CL training. However, few of the existing approaches address this issue in an unsupervised manner. To break through this wall, we introduce image information entropy (IIE), a derived form of information entropy, to estimate the complexity of a pixel with its neighboring content. With the aid of IIE, we can divide pixels into low-, medium-, and high-info groups and compare more contrastive pixel pairs in more informative regions.

Second, pixels contain different amounts of semantic information related to downstream tasks, resulting in different levels of effectiveness for contrastive learning according to the “InfoMin” principle [32]. Positive pairs in pixels with more semantic information will get hurt more in CL when having stronger augmentation. Stronger augmentation brings more perturbations in absolute value to positive pairs, and erodes the semantic information. Therefore, in this paper, we apply different strategies to different pixels: weaker augmentation for higher informative pixels and stronger augmentation for lower informative pixels.

In sum, we propose an **information-guided pixel augmentation** strategy for pixel-wise contrastive learning as in Fig. 1, with the following notable contributions:

- To the best of our knowledge, we are **the first** to propose a pixel augmentation method **with a pixel granularity** for enhancing unsupervised pixel-wise contrastive learning.
- We introduce the metric of **image information entropy** (IIE) to quantify the information a pixel contains. Guided by the IIE value, we then divide pixels into low-, medium-, and high-info groups and demonstrate the importance of high- and medium-info pixels in pixel-wise contrastive learning.
- We leverage **the “InfoMin” principle** and empirically prove its applicability to pixel-wise CL by using adaptive augmentation intensities for different groups of pixels, which leads to better experimental performances.
- We extensively validate the effectiveness of our core strategies that include the biased selection of high-info pixels and the use of adaptive augmentation strategies, which significantly enhances the one-shot model

CC2D [43] from 2.85mm to 2.31mm and 2.20mm to 1.70mm in MRE on Cephalometric and Hand X-ray datasets, respectively. Furthermore, it improves the performance of the state-of-the-art supervised landmark detection model ERE [25].

2. Related Work

2.1. Contrastive learning

Contrastive learning (CL) is one of the most powerful paradigms of self-supervised learning, leading to state-of-the-art performances in many vision tasks [7, 38, 47]. Most existing methods, like MoCo [6, 14], SimCLR [4, 5], BYOL [12] and BarlowTwins [49], are designed and optimized in instance-level comparisons, benefiting the trained model with more discriminative and generalizable representations. But such instance-level modeling leads to sub-optimal representations for downstream tasks requiring pixel-level prediction, *e.g.*, segmentation, object detection, and landmark detection. Recently some pixel-level methods attempt to learn dense feature representations [11, 41]. Xie *et al.* [41] propose an unsupervised pixel-level contrastive learning framework and achieve better performance on dense tasks like segmentation and detection. Multi-scale pixel-wise contrastive proxy task based on InfoNCE loss [13, 26] is introduced in [43] and achieves great performance in medical landmark detection, which is used for our feature extractor. Besides, some researchers introduce pixel-wise contrastive learning into supervised [36] or semi-supervised learning [1–3, 15, 16, 23, 35, 37, 39, 45, 46, 51, 52, 54] and succeed to improve their models. Other tasks [24, 40, 42, 44], such as weakly supervised methods also benefit greatly from the pixel-wise contrastive technique [10, 18]. However, to the best of our knowledge, none of them try to boost pixel-wise contrastive learning in an unsupervised manner.

2.2. Data augmentation

Data augmentation is the subject of extensive research today. It is also regarded as the process of generating different “views” from raw data in contrastive learning. Nowadays, researchers strive to create diverse views on various tasks in different ways. MixUp [19, 33, 48, 50] blends images and their labels in a paired style to strengthen supervised learning methods. Manifold MixUp [33] is designed for supervised learning, applying regularization on features, while Un-mix [31] recommends MixUp in the image/pixel space for self-supervised learning; i-Mix [20] regularizes the training progress in contrastive training by mixing instances in both the input and virtual label spaces. MoChi [17] proposes mixing the negative samples in the embedding space for hard negatives augmentation to help with CL models but hurt the classification accuracy. Zhu

et al. [56] mix both positive and negative samples to further create more views to boost CL. Besides, some other methods control the selection of views, such as Robinson *et al.* [29] select top-k hardest views as negative views. Some other researchers leverage the knowledge from annotations to generate views [23]. Liu *et al.* [23] sample positive views via confidence maps generated by semi-supervised models. Wang *et al.* [37] treat the pixels belonging to the same categories as positive pairs with the aid of segmentation masks. In this paper, we introduce IIE to guide the generation process of positive pairs in an unsupervised style, and apply adaptive augmentation to generate more various pixels for pixel-wise CL effectively.

3. Preliminaries

3.1. Contrastive learning setup

Contrastive learning aims to learn representation by clustering *positive pairs*, representing similar samples with the same semantic content, and discriminating *negative pairs*, representing dissimilar samples with different semantic content. Specifically, the positive pairs are often obtained from views generated from the same image with different augmentations. Similar to instance-wise CL, pixel-wise CL considers image patches at the identical location as positive pairs.

Let p_{data} be the data distribution and $p_{pos}(\cdot, \cdot)$ the distribution of positive pairs. We have *contrastive loss* (InfoNCE loss), which has been shown effective by many recent contrastive learning methods [26, 43], as follows:

$$\mathcal{L}_{\text{contrastive}}(f; \tau, M) = \mathbb{E}_{\substack{(x, x^+) \sim p_{pos} \\ \{\mathbf{x}_i^-\}_{i=1}^M \stackrel{\text{i.i.d.}}{\sim} p_{data}}} \left[-\log \frac{e^{f(\mathbf{x})^\top f(\mathbf{x}^+)/\tau}}{e^{f(\mathbf{x})^\top f(\mathbf{x}^+)/\tau} + \sum_{i=1}^M e^{f(\mathbf{x}_i^-)^\top f(\mathbf{x}^+)/\tau}} \right], \quad (1)$$

where f is the feature to be learned, $\tau > 0$ is a temperature hyper-parameter, and M is the number of negative samples.

3.2. Indicators

To better characterize pixels and their relationships, we hereby introduce three indicators: (1) Image Information Entropy (IIE); (2) Mutual information (MI).

Image Information Entropy (IIE). IIE is a metric introduced to quantify the information of a pixel using a small patch centered at this pixel in our method. For a specific pixel p , we crop a $k \times k$ patch X_p whose center locates at p , obtain the grayscale value distribution \mathcal{G} , and calculate the entropy of \mathcal{G} as the entropy of the pixel p .

$$H(p) = H(\mathcal{G}) = - \sum_{g \in \mathcal{G}} P(g) \log P(g) \quad (2)$$

Mutual information (MI). MI is a metric to assess the statistical relevance of two entities. Here we use MI to estimate the relevance of two patches of interest. In practice, similar to IIE, we first obtain the grayscale value distributions \mathcal{G}_p and \mathcal{G}_q of pixels p and q and then calculate the mutual information between \mathcal{G}_p and \mathcal{G}_q .

$$\hat{I}[p; q] = \sum_{y \in \mathcal{G}_q} \sum_{x \in \mathcal{G}_p} P_{\mathcal{G}_p, \mathcal{G}_q}(x, y) \log \left(\frac{P_{\mathcal{G}_p, \mathcal{G}_q}(x, y)}{P_{\mathcal{G}_p}(x) P_{\mathcal{G}_q}(y)} \right). \quad (3)$$

Compared with the contrastive loss which fluctuates along with the network training, MI is more stable and always gives a definite quantitative result for a particular pair.

3.3. Task description

In this study, we focus on a medical application of the local feature matching problem, used for medical landmark detection. We follow [28] to build our basic encoder, which is trained by pixel-wise contrastive learning. Specifically, in the training stage, two encoders F and F' with the same architecture are fed with the original image X and its augmented version X' , respectively. Next, the features from different encoders but with responses to the same corresponding pixel are matched to calculate the CL loss.

In the inference stage, we denote the set of points to match by $P = \{p_1, p_2, \dots, p_L\}$. Suppose that $p_l^T \in P^T$ is the l^{th} point in the template T , its corresponding p_l^X in the image X is found by the following *searching-and-maximizing* problem:

$$p_l^X = \arg \max_p s[F \circ T(p_l^T), F \circ X(p)]; p_l^T \in P^T, \quad (4)$$

where p is coordinates of a pixel, s is a similarity function, and $F \circ X(p)$ computes the feature map for the image X and then extracts the feature vector at pixel p . The goal of local feature matching is to accurately match points with semantic consistency. It should be noted that all analysis experiments presented below are conducted on the Cephalometric dataset [34].

4. Method

Pixels behave differently as shown in Figure 2, inspiring us to treat them with different strategies for each pixel. We naturally reform the standard contrastive loss into a pixel-wise adaptive loss:

$$\mathcal{L} = \sum_i \mathcal{L}_i(\rho_i, A_i) = \sum_i \rho_i \mathcal{L}(\tau(x_i, A_i), x_i), \quad (5)$$

where x_i refers to a pixel (along with its content in image patch), $\tau(x_i, A_i)$ refers to transformation on x_i with augmentation parameters A_i and ρ_i refers to the weights of x_i during training. However, the above ideal case of customizing strategies $\{\rho_i, A_i\}$ for each pixel x_i is hard to achieve

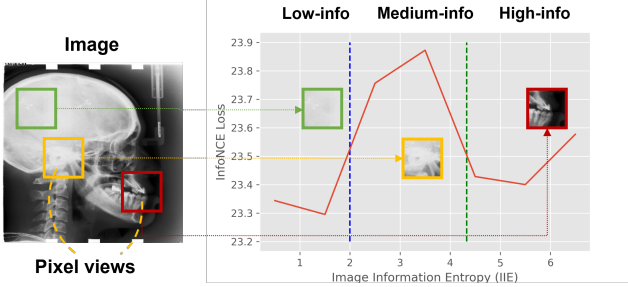


Figure 2. The curve of the contrastive loss (red line) against different IIE thresholds, which split pixels into three categories: low-info pixels (left of blue dashed line); medium-info pixels (between blue and green dashed lines); high-info pixels (right of green dashed line).

due to its time-consuming nature, thus a practical way is to cluster x_i into several classes and adjust $\{\rho, A\}$ for each class.

4.1. Information-guided pixel categorization

To cluster x_i , we use *Image Information Entropy* (IIE) and *contrastive loss* (Loss), which are already detailed in section 3. Figure 2 shows a U-shaped curve of the loss against IIE, nicely splitting pixels into three categories: low-, medium- and high-info pixels. We list their details as follows.

1. Low-info pixels featuring low IIE and low loss: most of them contain less semantic information and much noise (low IIE) but are easy to discriminate (low loss).
2. Medium-info pixels featuring medium IIE and high loss: they have medium texture information (medium IIE) but are hard to discriminate for networks (high loss).
3. High-info pixels featuring high IIE and low loss: most of them are edges and corners with much deterministic information (high IIE) and they are easy to discriminate for networks (low loss).

With the division of all pixels into three categories, our pixel augmentation goal can be formulated as follows:

$$\mathcal{L}(\rho_l, \rho_m, \rho_h, A_l, A_m, A_h) = \sum_{\alpha \in \{l, m, h\}} \rho_\alpha \mathcal{L}_\alpha(f(\tau(x_\alpha, A_\alpha), x_\alpha)), \quad (6)$$

where the total loss \mathcal{L} is split into 3 losses \mathcal{L}_l , \mathcal{L}_m and \mathcal{L}_h with their sampling ratios ρ_l , ρ_m , and ρ_h and augmentation intensities A_l , A_m , and A_h for the low-, medium- and high-info pixels x_l , x_m , and x_h , respectively. The proposed strategy of augmenting pixels is to find the optimal **sampling ratio** and **augmentation intensity** for each category

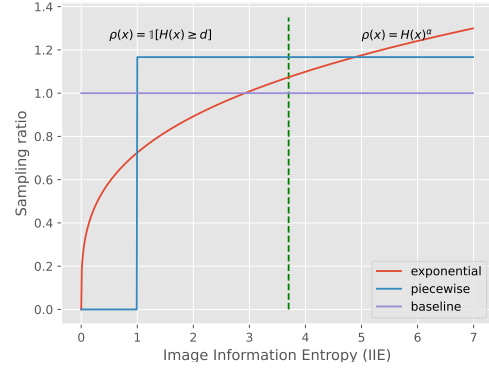


Figure 3. The green dashed line: entropy of all annotated landmarks are above this line. The violet line (baseline): sampling probability is same for all pixels. The red line: sampling probability of an entropy-based sampling weight map. Blue line: sampling probability of a piecewise weight map.

Exponential weight map						
γ	0	0.01	0.1	0.3	0.5	1.0
MRE	2.91	2.76	2.48	2.46	2.50	2.51
Piecewise weight map						
d	0	1	2	3	3.7	4.5
MRE	2.91	2.46	2.46	2.50	4.25	4.23

Table 1. Accuracy under different weight maps.

such that the overall loss is minimized. Next, we will elaborate how to do so one by one.

4.2. Sampling ratio

Per prior knowledge, medical landmarks, usually are localized at those meaningful points to guide clinical analysis; thus, it is natural to focus on high-info regions. In addition to this intuitive motivation, we also find that the loss of low-info pixels quickly reaches a low value and remains low even when the sampling rate of low-info pixels is reduced. Based on both intuitive and experimental findings, we propose to reduce ρ_l , thereby forcing the network to focus on medium- and high-info pixels.

When reducing ρ_l , there comes a natural question: *whether low-info areas are at all needed?* To explore it, we design two experimental schemes to analyze the pixels: (1) exponential weight map, $\rho(x) = H(x)^\gamma$; (2) piecewise weight map, $\rho(x) = \mathbb{1}[H(x) \geq d]$. For (1), we gradually increase the exponent γ of entropy weight map; For (2), we discard low-info pixel views x_l and gradually increase the threshold d between x_l and x_m (Figure 3). We empirically find that discarding a large amount of low-info pixel views is not advisable. As shown in Table 1, the pixels whose entropy is below 1 contain much less information and are actually useless for our model; the pixels whose entropy is between 1 and 3 contain both useful and useless

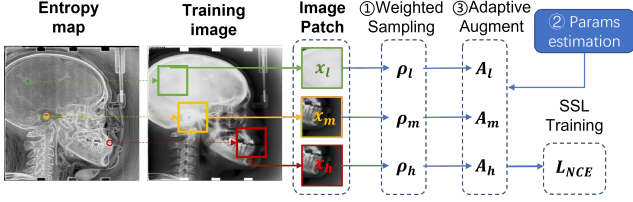


Figure 4. Pipeline of our method, consisting of 3 steps.

information; and the pixels whose entropy is greater than 3 are mostly useful. Considering the prior knowledge that the IIE values of ground truth landmarks in Cephalometric are almost greater than 3.7 (Green dashed line in Figure 3), some low-info pixels are kept to utilize their contributions to the variety of contrastive learning as they may contain the knowledge we need.

4.3. Augmentation intensity

After solving ρ in Eqn. (6), we then optimize A for each group of pixels by leveraging the “InfoMin” principle.

4.3.1 Minimal necessary shared information

To investigate optimal views for contrastive learning, Tian *et al.* [32] propose the “InfoMin” principle — *A good set of views are those that share the minimal information necessary to perform well at the downstream task* and give two definitions and a proposition as follows:

Given two random variables \mathbf{v}_1 and \mathbf{v}_2 , which are two views of the data x in practice, two encoders (f_1 for \mathbf{v}_1 and f_2 for \mathbf{v}_2) resulting representations $\mathbf{z}_1 = f_1(\mathbf{v}_1)$ and $\mathbf{z}_2 = f_2(\mathbf{v}_2)$, we have

Definition 1. (Sufficient Encoder) *The encoder f_1 of \mathbf{v}_1 is sufficient in the contrastive learning framework if and only if $I[\mathbf{v}_1; \mathbf{v}_2] = I[f_1(\mathbf{v}_1); \mathbf{v}_2]$. $I[\mathbf{v}_1; \mathbf{v}_2]$ denotes the mutual information between \mathbf{v}_1 and \mathbf{v}_2 . Generally speaking, a sufficient encoder refers to a well-trained encoder that can encode all necessary information relevant to tasks. In other words, the encoder f_1 is sufficient if \mathbf{z}_1 has kept all necessary information that the contrastive learning objective requires. Symmetrically, f_2 is sufficient if $I[\mathbf{v}_1; \mathbf{v}_2] = I[\mathbf{v}_1; f_2(\mathbf{v}_2)]$.*

Definition 2. (Minimal Sufficient Encoder) *A sufficient encoder f_1 of \mathbf{v}_1 is minimal if and only if $I[f_1(\mathbf{v}_1); \mathbf{v}_1] \leq I[f(\mathbf{v}_1); \mathbf{v}_1], \forall f$ that is sufficient. Among those encoders that are sufficient, the minimal ones, that only extract relevant information of the contrastive task and throw away other irrelevant information, are proved to be the most robust encoders, and also what we mainly care about.*

Proposition 1. *Suppose f_1 and f_2 are minimal sufficient encoders. Given a downstream task \mathcal{T} with label \mathbf{y} , the optimal views created from the data \mathbf{x} are $(\mathbf{v}_1^*, \mathbf{v}_2^*) = \arg \min_{\mathbf{v}_1, \mathbf{v}_2} I[\mathbf{v}_1; \mathbf{v}_2]$, subject to $I[\mathbf{v}_1; \mathbf{y}] = I[\mathbf{v}_2; \mathbf{y}] =$*

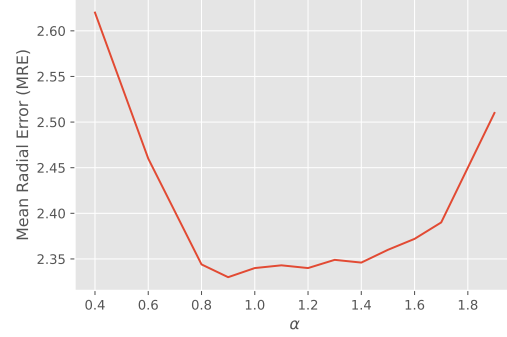


Figure 5. Model performance with different $\hat{\alpha}$.

$I[\mathbf{x}; \mathbf{y}]$. Given $\mathbf{v}_1^*, \mathbf{v}_2^*$, the representation \mathbf{z}_1^* (or \mathbf{z}_2^*) learned by contrastive learning is optimal for \mathcal{T} , thanks to the minimality and sufficiency of f_1 and f_2 . The above proposition states the importance of the pairs with minimal necessary shared information, which motivates us to find them in pixel-wise CL.

4.3.2 Augmentation intensity estimation

Inspired by the “InfoMin” principle, we can estimate our optimal augmentation parameters by minimizing the gap between the MI among augmented positive pairs and the minimal necessary MI among samples of the same class.

$$A = \arg \min_{A \in \mathcal{A}} \left\| \underbrace{\min\{I[\mathbf{v}; \mathbf{v}']\}}_{(a)} - \underbrace{\mathbb{E}\{\hat{I}[\mathbf{v}; \tau(\mathbf{v}, A)]\}}_{(b)} \right\|_1 \quad (7)$$

Two components are involved in Eqn. (7): (a) estimating minimal necessary MI; (b) estimating MI among augmented pairs.

Approximating minimal necessary MI: Due to the difficulty of directly obtaining the minimal necessary MI, an upper bound is proposed to approximate it as follows:

$$\begin{aligned} \min I[\mathbf{v}; \mathbf{v}'] &= \min_{\alpha} \alpha I[\mathcal{G}(\mathbf{v}); \mathcal{G}(\mathbf{v}')] \\ &\leq \mathbb{E}\{\alpha I[\mathcal{G}(\mathbf{v}); \mathcal{G}(\mathbf{v}'])\} \\ &\leq \hat{\alpha} \mathbb{E}\{\hat{I}[\mathbf{v}; \mathbf{v}']\}; \hat{\alpha} = \max(\alpha), \end{aligned} \quad (8)$$

where \mathbf{v} and \mathbf{v}' are views corresponding to an identical key point), $\mathcal{G}(\mathbf{v})$ is the grayscale value distribution of \mathbf{v} , and α denotes a scale factor. As it is hard to estimate the mutual information between images, the common alternative is to estimate the MI between the grayscale value distributions of images. However, the progression from \mathbf{v} to $\mathcal{G}(\mathbf{v})$ loses information due to dimensional reduction; we regard α as the inverse ratio of information loss.

With this approximation, Eqn. (7) can be rewritten into

$$A = \arg \min_{A \in \mathcal{A}} \mathbb{E}\left\{ \left\| \hat{\alpha} \hat{I}[\mathbf{v}; \mathbf{v}'] - \hat{I}[\mathbf{v}; \tau(\mathbf{v}, A)] \right\|_1 \right\} \quad (9)$$

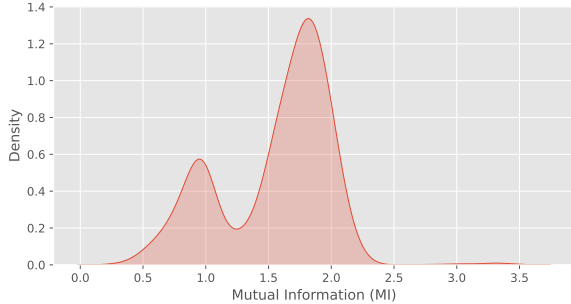


Figure 6. Probability density of mutual information among high-info pixels.

Details: Specifically, as demonstrated in Eqn. (10), we select k pixels as key points l from a randomly selected image X_0 in a particular group (low-, medium- or high-info). We calculate the necessary mutual information of key points of interest l_j by predicting the corresponding pixels l_j^i in each image X_i via a pre-trained encoder and then calculating mutual information between the corresponding patches located at key points. In addition, $\hat{\alpha}$ is considered as a hyper-parameter which will be analysed in ablation study. Finally, we can adjust the augmentation parameters A by increasing A iteratively to achieve our goal.

$$A = \arg \min_{A \in \mathcal{A}} \frac{1}{k} \left\{ \left\| \frac{\hat{\alpha}}{n} \sum_{j=1}^k \sum_{i=1}^n I[l_j; l_j^i] - \sum_j I[l_j; \tau(l_j, A)] \right\|_1 \right\}. \quad (10)$$

The distribution of $\hat{I}[l_j; l_j^i]$ is visualized in Figure 6. In practice, we estimate parameters for two augmentation operations that adjust image brightness and contrast, that is, $A = \{a_{br}, a_{ct}\}$. Based on the above, we can obtain augmentation parameters for all three groups, A_l , A_m , and A_h . **Adaptive augmentation:** After obtaining A_l , A_m , A_h , we can easily apply adaptive augmentation via Eqn. (6).

4.4. Method summary

Our methods can be concluded into 3 sequential steps as demonstrated in Figure 4 and Eqn. (6): (1) Reducing ρ_l by entropy-based sampling weight maps. (2) Estimating data augmentation parameters A_l , A_m , A_h by mutual information; and (3) Applying adaptive data augmentation.

5. Experiment

5.1. Datasets and Settings

Cephalometric dataset: It is a widely-used public dataset for cephalometric landmark detection, containing 400 radiographs, and is provided in IEEE ISBI 2015 Challenge [34]. There are 19 landmarks of anatomical significance labeled by 2 expert doctors in each radiograph. We

integrate the original two testsets into a combined testset. All analysis experiments are conducted on Cephalometric dataset.

Hand X-ray dataset: It is also a public dataset including 909 X-ray images of hands. The setting of this dataset follows [27]. The first 609 images are used for training and the rest for testing.

H&N 3D dataset: It is a 3D dataset constructed by Lei *et al.* [21] with landmarks marked via segmentation masks from a mixed head and neck (H&N) CT dataset.

Metrics: Following the official challenge [34], we use a mean radial error (MRE) to measure the Euclidean distance between prediction and ground truth, and successful detection rate (SDR) in four radii (2mm, 2.5mm, 3mm, and 4mm).

Model: We build our encoder following the SSL module of CC2D [43]. All model and training settings are the same as [43]. In addition, the one-shot template used for evaluation is selected by [28] in an unsupervised style.

Implementation details: All training and testing images are resized to 384×384 . We intuitively define $\{0, 2, 4\}$ as thresholds of low-, medium-, high-info groups. $\gamma = 0.3$ on Cephalometric dataset and $\gamma = 0.2$ in Hand X-ray and H&N 3D datasets. We set $\hat{\alpha}$ to 1 for all three datasets. The patch size k for estimating IIE is set to 10 for Cephalometric and Hand X-ray datasets, and 5 for H&N 3D dataset. The CT values in H&N 3D dataset are clipped into $[-200, 400]$.

5.2. Main results

To directly measure the performance of our encoder, we quantitatively compare our method and other latest methods, Zhu [56], MOCHI [17] and Un-mix [31] on the local feature matching problem (Section 3.3). Results are listed on Table 2. It should be noted that, we use the augmentation parameters estimated for high-info pixels by our method in Zhu [56], MOCHI [17] and Un-mix [31] for fair comparison. Our estimated augmentation parameters perform much better than the original parameters. Because our CL model consists of two independent encoders that do not share weights and are optimized by their own gradients, cross-fusing the features from two different projection spaces in [56] leads to performance degradation. MOCHI [17] leverages mixed negative features and hard example mining to concentrate more on negative views, but they ignore the influence of positive views. Un-mix [31] creates views by linear interpolation on the image level, lacking pixel-level augmentation. Compared with these methods, we increase the diversity at the pixel level with adaptive effective augmentation. Our method **consistently** outperforms other methods and greatly improves the baseline model by 0.57mm in MRE (from 2.91mm to 2.34mm, a **19.6% reduction**).

We also load these SSL weights as pretrained weights on several supervised models [25, 27, 55] as well as a one-

Table 2. Comparison of SSL for *local feature matching* with other approaches on Cephalometric [34] testset.

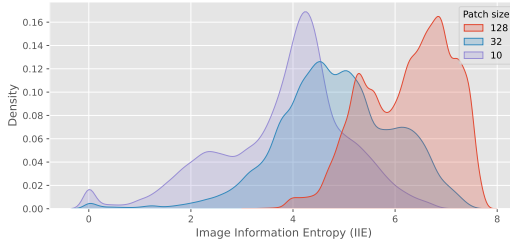
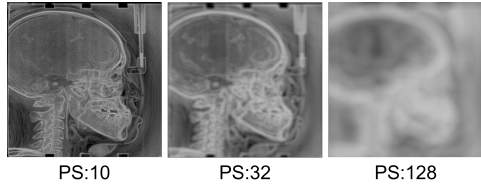
Method	MRE (\downarrow) (mm)	SDR (\uparrow) (%)			
		2mm	2.5mm	3mm	4mm
baseline	2.91	39.85	48.94	58.87	72.31
Zhu. [56]*	4.19 (+1.28)	24.35	32.38	42.66	60.10
MOCHI [17]*	2.56 (-0.35)	50.35	59.19	68.70	82.10
Un-mix [31]*	2.54 (-0.37)	44.82	56.48	67.57	83.87
Ours	2.34 (-0.57)	51.28	62.88	73.70	86.50

* using augmentation parameters estimated for high-info pixels by our method.

Table 3. Ablation study for components in our method on Cephalometric [34] testset.

Entr	Aug	MRE (\downarrow) (mm)	SDR (\uparrow) (%)			
			2mm	2.5mm	3mm	4mm
		2.91	39.85	48.94	58.87	72.31
✓		2.46 (-0.45)	43.72	54.65	66.48	82.65
	✓	2.41 (-0.50)	50.08	60.96	71.81	84.58
✓	✓	2.34 (-0.57)	51.28	62.88	73.70	86.50

Entr: entropy-based weight map; **Aug**: augmentation parameters estimation and adaptive augmentation.



PS	MRE (\downarrow)
10	2.34
32	2.37
128	2.39

Figure 7. Left: the IIE maps generated by different sizes of image patches; Middle: the probability density of IIE with different patch sizes; and Right: results with IIE maps of different patch sizes (PS).

shot models [43] and evaluate them on Cephalometric [34] and Hand-Xray datasets. It should be noted that CC2D consists of two stages, self- and semi-supervised learning modules. We apply our pre-trained model as the stage one model and then finetune on the semi-supervised model. As shown in Table 4, all models benefit from most pretrained models on MRE. In particular, models based on our SSL pretrained model achieve the largest improvement. Such an improvement is more prominent for one-shot model CC2D-S2. For example, when compared with the one-shot CC2D-S2 model that is based on a pretrained model from ImageNet, we reduce the MRE by 0.54mm (from 2.85mm to 2.21mm, a **22.4% reduction**) in the Cephalometric testset and by 0.52mm (from 2.22mm to 1.70mm, a **23.4% reduction**) in the Hand X-ray testset. In addition, some SDR values degrade because the pretrained model tends to optimize the bad cases and pay less attention to the good ones.

5.3. Ablation study

Components: Table 3 demonstrates the impact of each module. As shown in Table 3, both IIE mapping and adaptive augmentation with parameter estimation bring huge improvements to SSL training due to effective noise reduction and successfully unleashing the potential of each pixel. The IIE map greatly improves the baseline by 0.45mm in MRE, and the adaptive augmentation also helps to further improve the model by 0.12mm in MRE.

Hyperparameter $\hat{\alpha}$: Figure 5 demonstrates that $\hat{\alpha}$ close to 1 is a good choice. When α increases from 1, the model degenerates slowly; when α decreases from 0.8, the model

degenerates greatly. A too low $\hat{\alpha}$ is not recommended.

Generation of IIE maps: The generation of IIE maps is relevant to our method. Compared with a patch size of 10 (default in our method), larger patch sizes (32 and 128) lead to a smoother entropy graph (Figure 7(left)) and including more information increases the pixel’s entropy and results in a narrow range of IIE, thereby failing to capture local details important for landmark detection (Figure 7(middle)). The table in Figure 7(right) also demonstrates that IIE maps with larger patch sizes perform worse. The model degrades in MRE when the patch size increases from 10 to 32.

6. Conclusion

We propose an information-guided pixel augmentation strategy to boost pixel-wise CL. We first classify pixels into three categories, namely low-, medium-, and high-informative, based on the information quantity the pixel contains. Inspired by the “InfoMin” principle, we then design separate strategies for each category including: (1) sampling pixels with entropy-based weight maps; (2) estimating augmentation parameters by mutual information; (3) applying adaptive augmentation. Numerous experiments validate that our information-guided pixel augmentation strategy succeeds in encoding more discriminative representations and outperforms other competitive approaches in unsupervised local feature matching. Additionally, supervised models can also be enhanced by our pretrained model. We plan to investigate better estimation strategy to further close the gap between optimal augmentation parameters and our estimates.

Table 4. Comparison of the *supervised* and *one-shot* approaches with different pre-trained model on Cephalometric [34], Hand X-ray [27] and H&N 3D test sets. The **best** and the second-best performances are highlighted.

Cephalometric Test1+2							
Type	Model	Pretrain	MRE (\downarrow) (mm)	SDR (\uparrow) (%)			
				2 mm	2.5 mm	3 mm	4 mm
Supervised	U-Net [30]	Imagenet [9]	2.07	56.54	67.83	79.43	91.76
		Zhu [56]	1.96 (-0.11)	61.38	72.06	82.02	93.05
		MOCHI [17]	1.94 (-0.13)	62.03	73.51	84.02	93.18
		Un-mix [31]	1.94 (-0.13)	61.95	73.20	82.96	93.17
		ours	1.93 (-0.14)	61.51	72.84	<u>83.05</u>	93.38
		ours	1.93 (-0.14)	61.51	72.84	<u>83.05</u>	93.38
	ERE [25]*	Imagenet [9]	1.42	80.10	87.34	91.81	96.19
		Zhu [56]	1.41 (-0.01)	79.24	86.33	90.92	95.38
		MOCHI [17]	1.40 (-0.02)	79.98	86.95	91.14	95.90
		Un-mix [31]	1.41 (-0.01)	79.70	86.68	91.06	95.48
		ours	1.39 (-0.03)	80.15	<u>87.17</u>	<u>91.32</u>	95.89
		ours	1.39 (-0.03)	80.15	<u>87.17</u>	<u>91.32</u>	95.89
	GU ² -Net [55]*	None	1.34	83.01	88.82	93.09	97.34
		Zhu [56]	1.32 (-0.02)	83.26	89.01	93.04	<u>97.42</u>
		MOCHI [17]	1.31 (-0.03)	<u>83.47</u>	89.13	93.07	97.51
		Un-mix [31]	1.31 (-0.03)	83.45	89.47	93.30	97.13
		ours	1.28 (-0.06)	84.50	89.78	93.38	97.34
		ours	1.28 (-0.06)	84.50	89.78	93.38	97.34
One-shot	CC2D-S2 [43] [#]	Imagenet [9]	2.85	39.30	50.12	61.30	77.93
		Zhu [56]	2.87 (+0.02)	38.73	49.57	61.15	78.10
		MOCHI [17]	2.47 (-0.38)	46.06	57.74	70.14	86.33
		Un-mix [31]	2.44 (-0.41)	<u>49.81</u>	<u>60.92</u>	<u>71.70</u>	86.35
		ours	2.31 (-0.54)	52.10	63.20	73.45	86.73
		ours	2.31 (-0.54)	52.10	63.20	73.45	86.73
Hand X-ray Testset							
Supervised	U-Net [30]	Imagenet [9]	1.32	82.78	90.52	94.49	97.82
		Zhu [56]	1.30 (-0.02)	81.94	89.52	93.96	97.90
		MOCHI [17]	1.27 (-0.05)	85.29	91.63	95.11	98.08
		Un-mix [31]	1.29 (-0.03)	83.88	91.10	94.97	<u>98.15</u>
		ours	1.24 (-0.08)	84.48	91.33	95.09	98.36
		ours	1.24 (-0.08)	84.48	91.33	95.09	98.36
	ERE [25]*	Imagenet [9]	0.396	99.01	99.44	99.64	99.74
		Zhu [56]	0.381 (-0.015)	99.01	99.38	99.58	99.70
		MOCHI [17]	0.380 (-0.016)	99.02	99.41	99.56	95.71
		Un-mix [31]	0.380 (-0.016)	99.02	99.42	99.55	95.70
		ours	0.377 (-0.019)	99.04	<u>99.43</u>	99.58	99.71
		ours	0.377 (-0.019)	99.04	<u>99.43</u>	99.58	99.71
	GU ² -Net [55]*	Imagenet [9]	0.683	96.13	97.98	<u>98.77</u>	99.39
		Zhu [56]	0.684 (+0.001)	96.17	97.95	98.79	<u>99.44</u>
		MOCHI [17]	0.680 (-0.003)	96.20	98.00	98.75	99.44
		Un-mix [31]	0.681 (-0.002)	96.17	97.95	98.74	99.42
		ours	0.671 (-0.012)	96.21	98.04	98.72	99.43
		ours	0.671 (-0.012)	96.21	98.04	98.72	99.43
One-shot	CC2D-S2 [43] [#]	Imagenet [9]	2.22	56.90	70.90	78.30	86.90
		Zhu [56]	2.26 (+0.04)	63.47	72.28	78.26	86.07
		MOCHI [17]	2.03 (-0.19)	67.76	76.02	81.78	88.88
		Un-mix [31]	1.98 (-0.24)	68.35	77.02	82.73	89.57
		ours	1.70 (-0.52)	72.33	80.04	85.19	92.49
		ours	1.70 (-0.52)	72.33	80.04	85.19	92.49
H&N 3D Testset							
Type	Model	Pretrain	MRE (\downarrow) (mm)				
			Avg.	BS	MD	PL	PR
One-shot	CC2D-S2 [43] [#]	Imagenet [9]	<u>10.78</u>	7.70	16.30	<u>8.65</u>	<u>10.47</u>
		Zhu [56]	14.50 (+3.72)	7.47	18.17	16.96	15.43
		MOCHI [17]	13.05 (+2.27)	6.98	<u>15.27</u>	14.97	14.99
		Un-mix [31]	11.75 (+0.97)	7.31	15.18	12.32	12.22
		ours	10.10 (-0.68)	<u>7.12</u>	15.32	8.11	9.88
		ours	10.10 (-0.68)	<u>7.12</u>	15.32	8.11	9.88

*: re-running the official code with image size of 384 × 384. CC2D-S2 [43][#]: results of the 2nd stage of CC2D. Imagenet [9]: loading weights pretrained with Imagenet for backbone. BS: Brainstem; MD: Mandible; PL: Left parotid; PR: Right parotid.

References

- [1] Inigo Alonso, Alberto Sabater, David Ferstl, Luis Montesano, and Ana C Murillo. Semi-supervised semantic segmentation with pixel-level contrastive learning from a class-wise memory bank. In *Proceedings of the IEEE/CVF International Conference on Computer Vision*, pages 8219–8228, 2021. [2](#)
- [2] Krishna Chaitanya, Ertunc Erdil, Neerav Karani, and Ender Konukoglu. Contrastive learning of global and local features for medical image segmentation with limited annotations. In Hugo Larochelle, Marc’Aurelio Ranzato, Raia Hadsell, Maria-Florina Balcan, and Hsuan-Tien Lin, editors, *Advances in Neural Information Processing Systems 33: Annual Conference on Neural Information Processing Systems 2020, NeurIPS 2020, December 6-12, 2020, virtual*, 2020. [2](#)
- [3] Krishna Chaitanya, Ertunc Erdil, Neerav Karani, and Ender Konukoglu. Local contrastive loss with pseudo-label based self-training for semi-supervised medical image segmentation. *CoRR*, abs/2112.09645, 2021. [2](#)
- [4] Ting Chen, Simon Kornblith, Mohammad Norouzi, and Geoffrey E. Hinton. A simple framework for contrastive learning of visual representations. In *Proceedings of the 37th International Conference on Machine Learning, ICML 2020, 13-18 July 2020, Virtual Event*, volume 119 of *Proceedings of Machine Learning Research*, pages 1597–1607. PMLR, 2020. [1](#), [2](#)
- [5] Ting Chen, Simon Kornblith, Kevin Swersky, Mohammad Norouzi, and Geoffrey E Hinton. Big self-supervised models are strong semi-supervised learners. *Advances in neural information processing systems*, 33:22243–22255, 2020. [1](#), [2](#)
- [6] Xinlei Chen, Haoqi Fan, Ross Girshick, and Kaiming He. Improved baselines with momentum contrastive learning. *arXiv preprint arXiv:2003.04297*, 2020. [1](#), [2](#)
- [7] Ching-Yao Chuang, Joshua Robinson, Yen-Chen Lin, Antonio Torralba, and Stefanie Jegelka. Debaised contrastive learning. *Advances in neural information processing systems*, 33:8765–8775, 2020. [2](#)
- [8] Elijah Cole, Xuan Yang, Kimberly Wilber, Oisin Mac Aodha, and Serge Belongie. When does contrastive visual representation learning work? In *Proceedings of the IEEE/CVF Conference on Computer Vision and Pattern Recognition*, pages 14755–14764, 2022. [1](#)
- [9] Jia Deng, Wei Dong, Richard Socher, Li-Jia Li, Kai Li, and Li Fei-Fei. Imagenet: A large-scale hierarchical image database. In *2009 IEEE Computer Society Conference on Computer Vision and Pattern Recognition (CVPR 2009)*, 20-25 June 2009, Miami, Florida, USA, pages 248–255. IEEE Computer Society, 2009. [8](#)
- [10] Ye Du, Zehua Fu, Qingjie Liu, and Yunhong Wang. Weakly supervised semantic segmentation by pixel-to-prototype contrast. In *Proceedings of the IEEE/CVF Conference on Computer Vision and Pattern Recognition*, pages 4320–4329, 2022. [2](#)
- [11] Wouter Van Gansbeke, Simon Vandenhende, Stamatios Georgoulis, and Luc Van Gool. Unsupervised semantic segmentation by contrasting object mask proposals. In *2021 IEEE/CVF International Conference on Computer Vision, ICCV 2021, Montreal, QC, Canada, October 10-17, 2021*, pages 10032–10042. IEEE, 2021. [2](#)
- [12] Jean-Bastien Grill, Florian Strub, Florent Altché, Corentin Tallec, Pierre H. Richemond, Elena Buchatskaya, Carl Doersch, Bernardo Ávila Pires, Zhaohan Guo, Mohammad Gheshlaghi Azar, Bilal Piot, Koray Kavukcuoglu, Rémi Munos, and Michal Valko. Bootstrap your own latent - A new approach to self-supervised learning. In Hugo Larochelle, Marc’Aurelio Ranzato, Raia Hadsell, Maria-Florina Balcan, and Hsuan-Tien Lin, editors, *Advances in Neural Information Processing Systems 33: Annual Conference on Neural Information Processing Systems 2020, NeurIPS 2020, December 6-12, 2020, virtual*, 2020. [2](#)
- [13] Michael Gutmann and Aapo Hyvärinen. Noise-contrastive estimation: A new estimation principle for unnormalized statistical models. In Yee Whye Teh and D. Mike Titterton, editors, *Proceedings of the Thirteenth International Conference on Artificial Intelligence and Statistics, AISTATS 2010, Chia Laguna Resort, Sardinia, Italy, May 13-15, 2010*, volume 9 of *JMLR Proceedings*, pages 297–304. JMLR.org, 2010. [2](#)
- [14] Kaiming He, Haoqi Fan, Yuxin Wu, Saining Xie, and Ross Girshick. Momentum contrast for unsupervised visual representation learning. In *Proceedings of the IEEE/CVF conference on computer vision and pattern recognition*, pages 9729–9738, 2020. [1](#), [2](#)
- [15] Hanzhe Hu, Jinshi Cui, and Liwei Wang. Region-aware contrastive learning for semantic segmentation. In *Proceedings of the IEEE/CVF International Conference on Computer Vision*, pages 16291–16301, 2021. [2](#)
- [16] Xinrong Hu, Dewen Zeng, Xiaowei Xu, and Yiyu Shi. Semi-supervised contrastive learning for label-efficient medical image segmentation. In Marleen de Bruijne, Philippe C. Cattin, Stéphane Cotin, Nicolas Padoy, Stefanie Speidel, Yefeng Zheng, and Caroline Essert, editors, *Medical Image Computing and Computer Assisted Intervention - MICCAI 2021 - 24th International Conference, Strasbourg, France, September 27 - October 1, 2021, Proceedings, Part II*, volume 12902 of *Lecture Notes in Computer Science*, pages 481–490. Springer, 2021. [2](#)
- [17] Yannis Kalantidis, Mert Bulent Sariyildiz, Noe Pion, Philippe Weinzaepfel, and Diane Larlus. Hard negative mixing for contrastive learning. *Advances in Neural Information Processing Systems*, 33:21798–21809, 2020. [2](#), [6](#), [7](#), [8](#)
- [18] Tsung-Wei Ke, Jyh-Jing Hwang, and Stella X. Yu. Universal weakly supervised segmentation by pixel-to-segment contrastive learning. In *9th International Conference on Learning Representations, ICLR 2021, Virtual Event, Austria, May 3-7, 2021*. OpenReview.net, 2021. [2](#)
- [19] Sungnyun Kim, Gihun Lee, Sangmin Bae, and Se-Young Yun. Mixco: Mix-up contrastive learning for visual representation. *CoRR*, abs/2010.06300, 2020. [2](#)
- [20] Kibok Lee, Yian Zhu, Kihyuk Sohn, Chun-Liang Li, Jinwoo Shin, and Honglak Lee. i-mix: A domain-agnostic strategy for contrastive representation learning. In *9th International Conference on Learning Representations, ICLR 2021, Vir-*

- tual Event, Austria, May 3-7, 2021*. OpenReview.net, 2021. [2](#)
- [21] Wenhui Lei, Wei Xu, Ran Gu, Hao Fu, Shaoting Zhang, Shichuan Zhang, and Guotai Wang. Contrastive learning of relative position regression for one-shot object localization in 3d medical images. In *International Conference on Medical Image Computing and Computer-Assisted Intervention*, pages 155–165. Springer, 2021. [6](#)
- [22] David Liu, S. Kevin Zhou, Dominik Bernhardt, and Dorin Comaniciu. Search strategies for multiple landmark detection by submodular maximization. In *Computer Vision and Pattern Recognition (CVPR), 2010 IEEE Conference on*, pages 2831–2838. IEEE, 2010. [1](#)
- [23] Shikun Liu, Shuaifeng Zhi, Edward Johns, and Andrew J. Davison. Bootstrapping semantic segmentation with regional contrast. In *The Tenth International Conference on Learning Representations, ICLR 2022, Virtual Event, April 25-29, 2022*. OpenReview.net, 2022. [2, 3](#)
- [24] Yunze Liu, Li Yi, Shanghang Zhang, Qingnan Fan, Thomas A. Funkhouser, and Hao Dong. P4contrast: Contrastive learning with pairs of point-pixel pairs for RGB-D scene understanding. *CoRR*, abs/2012.13089, 2020. [2](#)
- [25] James McCouat and Irina Voiculescu. Contour-hugging heatmaps for landmark detection. In *Proceedings of the IEEE/CVF Conference on Computer Vision and Pattern Recognition (CVPR)*, pages 20597–20605, June 2022. [2, 6, 8](#)
- [26] Aaron van den Oord, Yazhe Li, and Oriol Vinyals. Representation learning with contrastive predictive coding. *arXiv preprint arXiv:1807.03748*, 2018. [2, 3](#)
- [27] Christian Payer, Darko Štern, Horst Bischof, and Martin Urschler. Integrating spatial configuration into heatmap regression based cnns for landmark localization. *Medical Image Analysis*, 54:207–219, 2019. [6, 8](#)
- [28] Quan Quan, Qingsong Yao, Jun Li, and S Kevin Zhou. Which images to label for few-shot medical landmark detection? In *Proceedings of the IEEE Conference on Computer Vision and Pattern Recognition*, 2022. [3, 6](#)
- [29] Joshua Robinson, Ching-Yao Chuang, Suvrit Sra, and Stefanie Jegelka. Contrastive learning with hard negative samples. *arXiv preprint arXiv:2010.04592*, 2020. [3](#)
- [30] Olaf Ronneberger, Philipp Fischer, and Thomas Brox. U-net: Convolutional networks for biomedical image segmentation. In Nassir Navab, Joachim Hornegger, William M. Wells III, and Alejandro F. Frangi, editors, *Medical Image Computing and Computer-Assisted Intervention - MICCAI 2015 - 18th International Conference Munich, Germany, October 5 - 9, 2015, Proceedings, Part III*, volume 9351 of *Lecture Notes in Computer Science*, pages 234–241. Springer, 2015. [8](#)
- [31] Zhiqiang Shen, Zechun Liu, Zhuang Liu, Marios Savvides, Trevor Darrell, and Eric Xing. Un-mix: Rethinking image mixtures for unsupervised visual representation learning. In *Proceedings of the AAAI Conference on Artificial Intelligence*, volume 36, pages 2216–2224, 2022. [2, 6, 7, 8](#)
- [32] Yonglong Tian, Chen Sun, Ben Poole, Dilip Krishnan, Cordelia Schmid, and Phillip Isola. What makes for good views for contrastive learning? *Advances in Neural Information Processing Systems*, 33:6827–6839, 2020. [1, 2, 5](#)
- [33] Vikas Verma, Alex Lamb, Christopher Beckham, Amir Najafi, Ioannis Mitliagkas, David Lopez-Paz, and Yoshua Bengio. Manifold mixup: Better representations by interpolating hidden states. In Kamalika Chaudhuri and Ruslan Salakhutdinov, editors, *Proceedings of the 36th International Conference on Machine Learning, ICML 2019, 9-15 June 2019, Long Beach, California, USA*, volume 97 of *Proceedings of Machine Learning Research*, pages 6438–6447. PMLR, 2019. [2](#)
- [34] Ching-Wei Wang, Cheng-Ta Huang, Jia-Hong Lee, Chung-Hsing Li, Sheng-Wei Chang, Ming-Jhih Siao, Tat-Ming Lai, Bulat Ibragimov, Tomaž Vrtovec, Olaf Ronneberger, et al. A benchmark for comparison of dental radiography analysis algorithms. *Medical Image Analysis*, 31:63–76, 2016. [3, 6, 7, 8](#)
- [35] Tao Wang, Jianglin Lu, Zhihui Lai, Jiajun Wen, and Heng Kong. Uncertainty-guided pixel contrastive learning for semi-supervised medical image segmentation. In Luc De Raedt, editor, *Proceedings of the Thirty-First International Joint Conference on Artificial Intelligence, IJCAI 2022, Vienna, Austria, 23-29 July 2022*, pages 1444–1450. ijcai.org, 2022. [2](#)
- [36] Wenguan Wang, Tianfei Zhou, Fisher Yu, Jifeng Dai, Ender Konukoglu, and Luc Van Gool. Exploring cross-image pixel contrast for semantic segmentation. In *2021 IEEE/CVF International Conference on Computer Vision, ICCV 2021, Montreal, QC, Canada, October 10-17, 2021*, pages 7283–7293. IEEE, 2021. [2](#)
- [37] Wenguan Wang, Tianfei Zhou, Fisher Yu, Jifeng Dai, Ender Konukoglu, and Luc Van Gool. Exploring cross-image pixel contrast for semantic segmentation. In *Proceedings of the IEEE/CVF International Conference on Computer Vision*, pages 7303–7313, 2021. [2, 3](#)
- [38] Xiao Wang and Guo-Jun Qi. Contrastive learning with stronger augmentations. *IEEE Transactions on Pattern Analysis and Machine Intelligence*, 2022. [2](#)
- [39] Jinxi Xiang, Zhuwei Li, Wenji Wang, Qing Xia, and Shaoting Zhang. Self-ensembling contrastive learning for semi-supervised medical image segmentation. *CoRR*, abs/2105.12924, 2021. [2](#)
- [40] Yutong Xie, Jianpeng Zhang, Zehui Liao, Yong Xia, and Chunhua Shen. PGL: prior-guided local self-supervised learning for 3d medical image segmentation. *CoRR*, abs/2011.12640, 2020. [2](#)
- [41] Zhenda Xie, Yutong Lin, Zheng Zhang, Yue Cao, Stephen Lin, and Han Hu. Propagate yourself: Exploring pixel-level consistency for unsupervised visual representation learning. In *IEEE Conference on Computer Vision and Pattern Recognition, CVPR 2021, virtual, June 19-25, 2021*, pages 16684–16693. Computer Vision Foundation / IEEE, 2021. [2](#)
- [42] Ke Yan, Jinzheng Cai, Dakai Jin, Shun Miao, Dazhou Guo, Adam P. Harrison, Youbao Tang, Jing Xiao, Jingjing Lu, and Le Lu. SAM: self-supervised learning of pixel-wise anatomical embeddings in radiological images. *IEEE Trans. Medical Imaging*, 41(10):2658–2669, 2022. [2](#)
- [43] Qingsong Yao, Quan Quan, Li Xiao, and S Kevin Zhou. One-shot medical landmark detection. In *International Confer-*

- ence on Medical Image Computing and Computer-Assisted Intervention*, pages 177–188. Springer, 2021. 2, 3, 6, 7, 8
- [44] Chenyu You, Weicheng Dai, Fenglin Liu, Haoran Su, Xiaoran Zhang, Lawrence Staib, and James S Duncan. Mine your own anatomy: Revisiting medical image segmentation with extremely limited labels. *arXiv preprint arXiv:2209.13476*, 2022. 2
- [45] Chenyu You, Weicheng Dai, Lawrence Staib, and James S Duncan. Bootstrapping semi-supervised medical image segmentation with anatomical-aware contrastive distillation. *arXiv preprint arXiv:2206.02307*, 2022. 2
- [46] Chenyu You, Ruihan Zhao, Lawrence H. Staib, and James S. Duncan. Momentum contrastive voxel-wise representation learning for semi-supervised volumetric medical image segmentation. In Linwei Wang, Qi Dou, P. Thomas Fletcher, Stefanie Speidel, and Shuo Li, editors, *Medical Image Computing and Computer Assisted Intervention - MICCAI 2022 - 25th International Conference, Singapore, September 18-22, 2022, Proceedings, Part IV*, volume 13434 of *Lecture Notes in Computer Science*, pages 639–652. Springer, 2022. 2
- [47] Yuning You, Tianlong Chen, Yongduo Sui, Ting Chen, Zhangyang Wang, and Yang Shen. Graph contrastive learning with augmentations. *Advances in Neural Information Processing Systems*, 33:5812–5823, 2020. 2
- [48] Sangdoon Yun, Dongyoon Han, Seong Joon Oh, Sanghyuk Chun, Junsuk Choe, and Youngjoon Yoo. Cutmix: Regularization strategy to train strong classifiers with localizable features. In *International Conference on Computer Vision (ICCV)*, 2019. 2
- [49] Jure Zbontar, Li Jing, Ishan Misra, Yann LeCun, and Stéphane Deny. Barlow twins: Self-supervised learning via redundancy reduction. In Marina Meila and Tong Zhang, editors, *Proceedings of the 38th International Conference on Machine Learning, ICML 2021, 18-24 July 2021, Virtual Event*, volume 139 of *Proceedings of Machine Learning Research*, pages 12310–12320. PMLR, 2021. 2
- [50] Hongyi Zhang, Moustapha Cisse, Yann N. Dauphin, and David Lopez-Paz. mixup: Beyond empirical risk minimization. *International Conference on Learning Representations*, 2018. 2
- [51] Xiangyun Zhao, Raviteja Vemulapalli, Philip Andrew Mansfield, Boqing Gong, Bradley Green, Lior Shapira, and Ying Wu. Contrastive learning for label efficient semantic segmentation. In *Proceedings of the IEEE/CVF International Conference on Computer Vision*, pages 10623–10633, 2021. 2
- [52] Yuanyi Zhong, Bodi Yuan, Hong Wu, Zhiqiang Yuan, Jian Peng, and Yu-Xiong Wang. Pixel contrastive-consistent semi-supervised semantic segmentation. In *2021 IEEE/CVF International Conference on Computer Vision, ICCV 2021, Montreal, QC, Canada, October 10-17, 2021*, pages 7253–7262. IEEE, 2021. 2
- [53] S. Kevin Zhou. Medical image recognition, segmentation and parsing: Machine learning and multiple object approaches, 2015. 1
- [54] Yanning Zhou, Hang Xu, Wei Zhang, Bin Gao, and Pheng-Ann Heng. C3-semiseg: Contrastive semi-supervised segmentation via cross-set learning and dynamic class-balancing. In *Proceedings of the IEEE/CVF International Conference on Computer Vision*, pages 7036–7045, 2021. 2
- [55] Heqin Zhu, Qingsong Yao, Li Xiao, and S Kevin Zhou. You only learn once: Universal anatomical landmark detection. In *International Conference on Medical Image Computing and Computer-Assisted Intervention*, pages 85–95. Springer, 2021. 6, 8
- [56] Rui Zhu, Bingchen Zhao, Jingen Liu, Zhenglong Sun, and Chang Wen Chen. Improving contrastive learning by visualizing feature transformation. In *Proceedings of the IEEE/CVF International Conference on Computer Vision*, pages 10306–10315, 2021. 3, 6, 7, 8